Monitoring X-ray Binary Pulsars with Fermi/GBM

P. A. Jenke[1] and C. A. Wilson-Hodge[2]

[1] University of Alabama in Huntsville, Huntsville, AL 35812, USA
[2] NASA, Marshall Space Flight Center, Huntsville, AL 35812, USA
E-mail(PJ): peter.a.jenke@nasa.gov

Abstract

The Fermi Gamma ray Burst Monitor (GBM) is a unique instrument that offers the largest instantaneous field of view of any hard X-ray instrument currently in operation. This capability along with excellent timing resolution, makes it very successful at detecting rare transient events as well as providing long integration times for pulsed signal extraction. Even though GBM has a relatively modest size, we are able to observe a typical accreting pulsar for over 40,000 seconds each day allowing us to make precise measurements of the source frequency and pulsed flux for sources with a spin frequency between 0.001 and 2 Hz. These frequency measurements due to GBM's excellent timing capabilities have given us the capability to determine/update orbital ephemerides for many sources as well as monitor rare torque reversals in persistent (semi-persistent) sources such as EXO 2030+375. Continuous Time Tagged Event data, available since November 2012, allows the GBM pulsar monitor to track the frequency of even higher frequency sources and we plan to make these histories available this year.

Key words: pulsars,neutron stars

1. Introduction

Using the Gamma ray Burst Monitor (GBM), the GBM Pulsar Monitoring program (GPM) is designed to monitor the frequency and pulsed flux of accreting pulsars and detect new outbursts from transient pulsars with spin periods between 0.5 to 1000 seconds and in the energy range between 8 and 50 keV. GBM is not an imaging instrument but has the advantage of observing the entire unocculted sky at all times with the exception of brief transverses of the South Atlantic Anomaly. This full sky coverage enables long term monitoring of accreting pulsars, allowing precise measurements of spin frequencies, pulsed flux, orbital parameters enabling studies of the flow of angular momentum from the donor star onto the neutron star and constraints on the magnetic field. The long source exposures possible with GBM are crucial for precise timing measurements, where the error on pulse frequency and pulse frequency rate estimates scale as $T^{-3/2}$ and $T^{-5/2}$, respectively, where T is the observation duration.

The pulsar monitor has a sister program, the GBM Earth Occultation Monitor (GEOM), which uses the fall and rise of the count rate of known sources as they are occulted by the Earth's limb and reappear again (Wilson-Hodge et al. 2012). This program is currently monitoring over 200 sources and is able to provide flux histories for these sources in the energy range between 8 and 300 keV. A spin-off program, the X-ray Burst (XRB) monitor uses the pulsar monitor's data cleaning process to identify thermonuclear type 1 XRBs from low $\dot{M}$ accreting neutron stars and has identified 752 photospheric radius expansion (PRE) burst in its first three years of operation starting in March 2010 (Jenke et al. 2016).

1.1. Gamma Ray Burst Monitor

GBM consists of 12 NaI detectors with a diameter of 12.7 cm and a thickness of 1.27 cm and two BGO detectors with a diameter and thickness of 12.7 cm. The NaI detectors have an energy range from 8 keV to 1 MeV, while the BGOs extend the energy range to 40 MeV. There are three continuous publicly available data types: CTIME data which has 8 energy channels (8–1000 keV for NaIs) with 256 ms timing resolution and is primarily used for localization and long event searches, CSPEC data which has 128 channels (8–1000 keV for NaIs) with 4,096 s timing resolution and is primarily used for spectroscopy, and CTTE data which has 128 channels (8–1000 keV for NaIs) with time tagged photon events with 2 μs precision and is used for spectroscopy, timing, and short interval searches. The pulsar monitor primarily uses CTIME data but is expanding its capability with CTTE data which increases sensitivity for higher frequency pulsars and improves pulsed spectral resolution for bright sources.

2. GBM Pulsar Monitor

The pulsar monitor consists of two efforts: (1) The daily blind search aims at detecting new pulsed transients and outbursts from known transients. (2) The dedicated search is currently monitoring the pulsed flux and frequency of 39 sources and has pulsed flux and frequencies histories for 36 detected sources. GPM is providing, through its website[1], quick-look estimates of pulsed flux and frequency for use in multi-wavelength observations. The website is updated twice a week and announcements of new outbursts from transient sources are published in Astronomer's Telegrams to facilitate follow-up observations.

2.1. Pulsed Searches with GBM

The analysis of GBM observations of pulsars presents two main challenges: the background rates are normally much larger than the source rates, and have large variations; and the responses of the detectors to a source are continuously changing because of Fermi's ever changing orientation. GPM meets these challenges with an empirical background subtraction and extensive on the fly calculations of detector response matrices. The initial step in our analysis consists of screening the NaI detector count rate data to remove phosphorescence events, gamma-ray burst and particle events and intervals of rapid spacecraft rotation. Then an empirical background model is fit to the rates and subtracted off, after which the rates are combined over detectors in a way that results in an estimate of the variable part of the source flux. From these flux variation estimates we conduct searches for pulsations, and monitor detected sources.

2.2. Empirical Background Subtraction

The screened rates in each channel of the 12 NaI detectors are fit with a model with that includes components for a small number of bright sources and a stiff empirical model that contains the low frequency component of the remaining rates. The source models are computed from a model flux spectrum using time dependent response matrices. One fit is made for each channel with the normalization factors for the bright sources common to all detectors, but with the stiff model parameters (a statistically constrained spline) independent for each detector. The model accounts for the occultation steps for the bright sources and the variation of the background due to spacecraft motion while upon subtraction retains the higher frequency signals of the frequency modulated sources.

2.3. Daily Blind Search

Using the background subtracted data, time dependent responses and a generic pulsar spectrum (power law with a high energy cut-off), source fluxes (8–50 keV) are determined for 26 directions along the Galactic plane (15 degree cadence) plus the LMC and SMC. The source fluxes are Fourier transformed and searched for significant pulsations. The peak frequencies and directions are determined by interpolating over the two dimensional grid of Fourier power and directions. A catalog of accreting pulsars with the last known spin frequency is compared with the peak frequency and direction in order to identify the pulsed signal. Significant unidentified pulsed signals are flagged for additional analysis. Additional analysis is limited by GBM's large location uncertainty (a few degrees) but typically includes searching for significant pulsations from a grid of directions that include higher latitudes and searching for new flaring pulsars in the MAXI X-ray monitor (Matsuoka. et al. 2009) and Swift BAT Hard X-ray Transient Monitor (Krimm et al. 2013).

2.4. Dedicated Search

In the dedicated search, source fluxes (8–50 keV) are similarly determined for the specific monitored pulsar position and energy spectrum of the source of interest. Appropriate lengths of data (usually a minimum of 5–10 times the pulse period) are fit to a Fourier expansion in pulse phase using a course phase model. Times are barycentered using the JPL Planetaria ephemeris DE200 (Standish 1990) and, if an ephemeris is available, corrected for orbital motion. Fourier components for short intervals (suitable for the source but usually a few days) are combined and searched for significant pulsations in up to three harmonics over a small range of frequency and possibly frequency derivative. This provides higher sensitivity than the blind searches because of the smaller search ranges and the use of source specific information such as the location, orbital parameters and flux spectrum.

GBM pulsar monitor currently has frequency histories and pulsed fluxes for 36 accreting binaries including 28 transients. Figure 2 lists the currently detected transients, most of which are Be X-ray binaries, and the times which GBM detects them. Of particular interest is the recent outburst of SMC X-3 in July 2016 (see Figure 1), currently the only SMC source GBM detects. EXO 2030+375 is GBM's most persistent transient source. Until recently, the GBM pulsar monitor has detected an outburst almost every periastron passage. The Be X-ray binary's spin-up flattened and the source faded from detection for 5 orbital periods in April 2016. When it reemerged on MJD 57632, the source had undergone a rare torque reversal. Surprisingly, after two more orbits, EXO 2030+375 appears to have resumed its previous spin-up state (see Figure 3).

*[1] https://gammaray.msfc.nasa.gov/gbm/science/pulsars.html

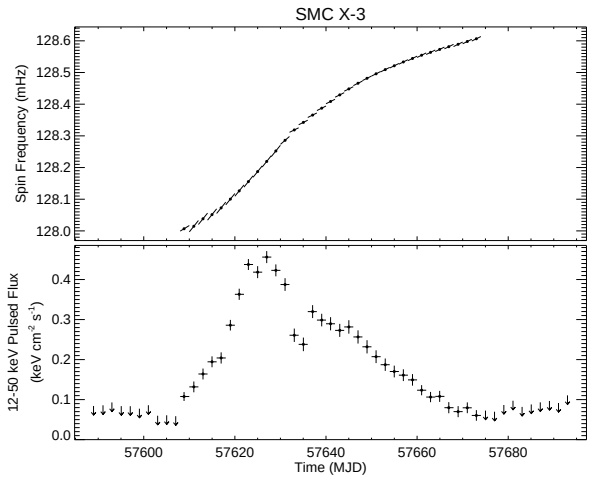

Fig. 1. The top panel is the frequency history of SMC X-3 while the bottom panel is the 12–50 keV pulsed flux. The frequencies have been corrected for orbital motion using the ephemeris from Townsend et al. (2017). Arrows indicate upper limits and the diagonal bars through the frequency points represent the best frequency derivative.

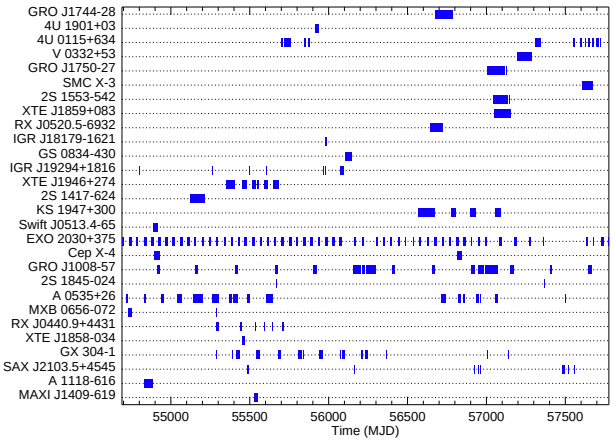

Fig. 2. The GBM detected transients are listed vertically while the times where they are detected are indicated by the blue bars.

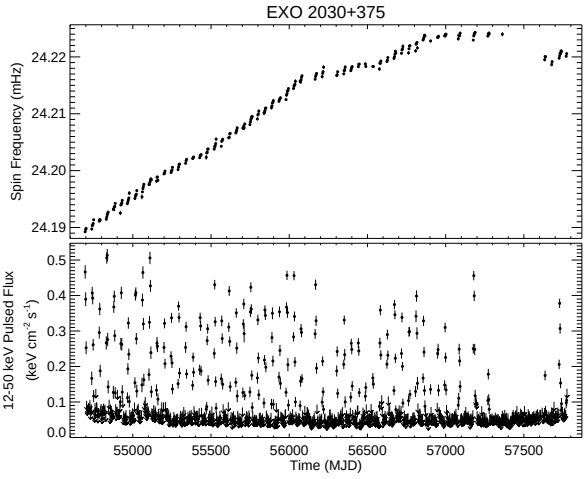

Fig. 3. The top panel is the frequency history of EXO 2030+375 while the bottom panel is the 12–50 keV pulsed flux. Arrows indicate upper limits. Notice the torque reversal and recovery around MJD 57300.

2.5. Orbital Ephemeris Determination

Typically, after correcting the pulse arrival times for Earth's motion, one can use the doppler boosted frequencies of the pulses to fit a model for the binary system for a source of interest. Material accreted onto a neutron star surface or collected in an accretion disk threaded by the neutron star's magnetic field transfers angular momentum to the neutron star. Disentangling this intrinsic spin-up from the orbital signature is challenging. A solution to this problem is to model the intrinsic spin-up using a proxy for the system's X-ray luminosity. The luminosity is a function of mass accretion which is related to the torque imposed on the neutron star. Rappaport & Joss (1977) showed that, at high luminosity, the intrinsic spin-up, $\dot{\nu}$, is proportional to $L^{6/7}$ when accretion is mediated through a disk. The proportionality constant is a function of mass, radius, moment of inertia, distance and magnetic field of the neutron star along with a few parameters describing accretion and emission efficiency. When connecting multiple outbursts with the same torque model, it is necessary to include a spin-down term to account for angular momentum losses during quiescence (see Figure 4).

A search for frequency and frequency rate is performed using pulse profiles from GBM folded over a multi–day interval. Each frequency epoch is chosen as the mean exposure–weighted observation time. The epochs are barycentered using the JPL Planetary ephemeris DE200 (Standish 1990). BAT survey data (15–50 keV) or MAXI X-ray data (10–20 keV) for the individual source is used as a proxy for the source luminosity and to model the intrinsic spin-up rate. This spin-up model along with the line of sight delay associated with the binary orbit from Deeter et al. (2003) is used to model the barycentered arrival times. Minimization of the χ^2 fit of the barycentric frequencies and the count rates (Swift/BAT or MAXI) is performed using the Levenberg-Marquart method and is of the form:

$$\chi^2 = \sum_i (f_i - (\dot{\nu}_i(1-\beta_i))^2 \quad ; i = 0, n-1 \qquad (1)$$
$$+ \sum_i (X_i - \dot{\nu}_i/m)^2 \quad ; i = 0, n-2 \qquad (2)$$

- β_i is the orbital redshift factor at time t_i which is a function of the orbital elements.
- f_i is the measured barycentric frequency at time t_i which is the frequency epoch of the search interval

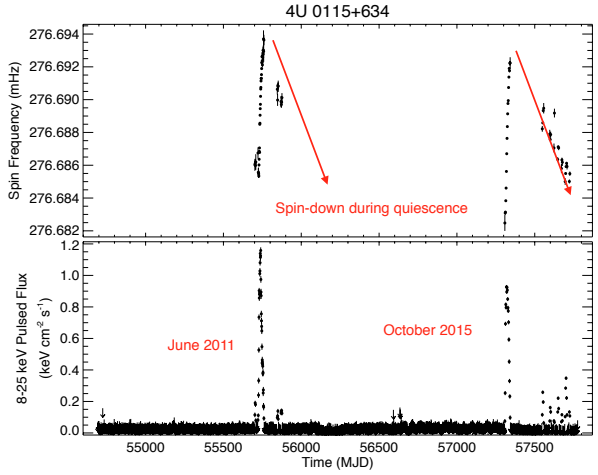

Fig. 4. The top panel is the frequency history of 4U 0115+634 while the bottom panel is the 8–25 keV pulsed flux. The frequencies have been corrected for orbital motion. There are two giant outbursts in June 2011 and October 2015 where there is significant spin-up do to accretion torques. After the giant outbursts, the pulsar spins down until a regular outburst occurs and there is again spin-up do to accretion torques although the spin-up is not as severe. Even between the normal outbursts there is significant spin-down (red arrows) which is modeled as 1 or 2 degree polynomial when fitting the frequencies to an orbital model.

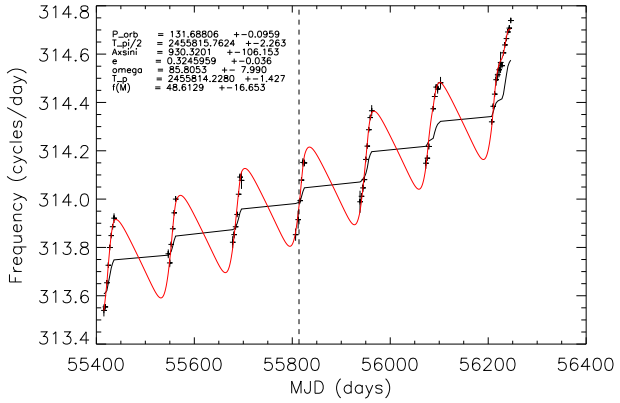

Fig. 5. Black points are the barycentered frequencies for GX 304−1. The black curve is the best fit torque model from the Swift/BAT rates while the red curve is the orbital model combined with the torque model. Notice how well the torque model represents the torque during the onset of the giant outburst at MJD 56200.

i. Each epoch, t_i, is chosen as the mean exposure-weighted observation time.

- X_i is the average value of $R^{6/7}$ between t_i and t_{i+1} and R is the MAXI count rate.
- The model parameter ν_i is the orbitally corrected frequency at time t_i and $\dot{\nu}_i$ is $(\nu_{i+1} - \nu_i)/(t_{i+1} - t_i)$.

The updated orbital model is used in a new search for frequencies and frequency rates recursively until the orbital solution becomes stationary. Figure 5 demonstrates this technique. Notice how well the torque model follows the transition between a normal and giant outburst around MJD 56200.

2.5.1. Long Term Monitoring

Combining GBM data with data from the pulsar monitor's predecessor which used data from the Burst and Transient Source Experiment (BATSE) on board the Compton Gamma Ray Observatory (CGRO), long term pulsed histories spanning twenty years may be created although there is a significant time gap between CGRO and the Fermi mission. Searches for orbital decay are possible by determining the orbital epoch at intervals over a long period of time. This is important for understanding how different X-ray binary populations might be related through evolution. Orbital solutions are determined where the source of interest was bright for the available BATSE and GBM data. The $T_{\pi/2}$ epoch is expanded in orbit number, n,

$$T_{\pi/2} = T_o + nP_{orb} + \frac{1}{2}n^2 P_{orb}\dot{P}_{orb}, \quad (3)$$

and the quadratic term determines the orbital decay of the source. The expected linear trend in the orbital epoch is subtracted and the residuals are fit to a quadratic polynomial corresponding to the last term in Eq 3 (See Figure 6). Significant orbital decay ($\dot{P} = (-9.74 \pm 0.77) \times 10^{-8}$) was detected in the wind fed high mass X-ray binary OAO 1657−414 (Jenke et al. 2012).

3. GBM Earth Occultation Monitor

The Earth occultation technique (EOT) measures the change in flux when a source enters (or exits) Earth occultation (see Figure 7). The occultation time must be known so a catalog of sources is used and updated regularly. The changing GBM detector response, atmospheric transmission, the source spectrum, and other sources also occulting within a four minute fit window (including the flaring Sun) are taken into account. The EOT is the only technique currently available that enables GBM to monitor persistent and transient galactic and extragalactic sources on timescales of days to years.

GEOM is currently monitoring 247 sources and light curves (12–300 keV in four energy bands) and fits files (12–1000 keV in six energy bands) are available on

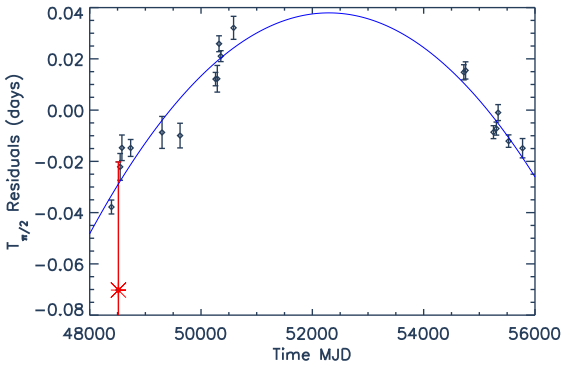

Fig. 6. Diamonds are orbital epochs for each ephemeris with a linear trend removed. The curve is a quadratic fit to the epochs. The residual epochs to the left are calculated from BATSE data while the residual epochs on the right are calculated from GBM data.

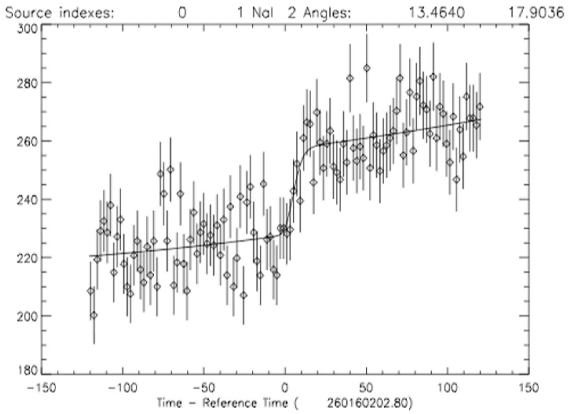

Fig. 7. Example of an occultation fit window. The occultation step for the source is clearly seen at t=0. The best model for the fit window is shown by the solid curve.

the web site[2]. GEOM has confidently detected over 100 of its monitored sources with 9 sources being detected ($> 5\sigma$) above 100 keV (Case et al. 2011). The sources detected above 100 keV include 7 persistent and 2 transient sources: the Crab, the BHs Cyg X-1, Swift J1753.5−0127, GRS 1915+105, 1E 1740−29, and GRS 1758−258, the AGN Cen A, and the transient BHs XTE J1752−223 and GX 339−4. We have also detected brief, bright events with single Earth occultations including numerous solar flares, and a brief episode of enhanced persistent emission from SGR 1550−5418.

GEOM compliments the GPM by monitoring transient outbursts of Galactic accreting binaries and measure the total flux of the source. GEOM can also monitor spectral changes in these systems which may accompany a change in the accretion state especially in bright black hole binaries such as Cyg X-1 (see Figure 8).

*2 https://gammaray.msfc.nasa.gov/gbm/science/earth_occ.html

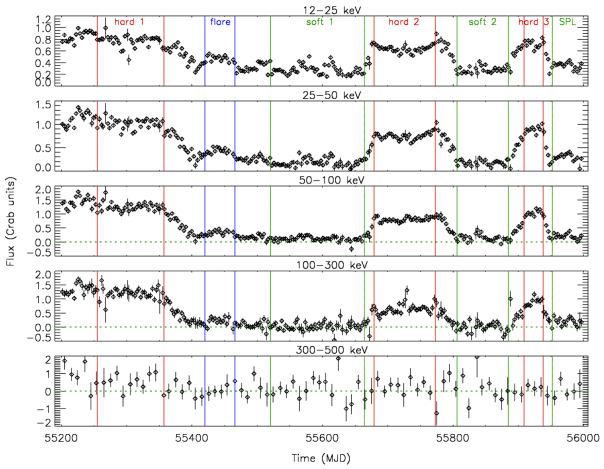

Fig. 8. GEOM results monitoring the flux for Cygnus X-1 shown for 12–25, 25–50, 40–100, 100–300, 300–500 keV energy bands. The vertical colored lines indicate times of state changes.

4. GBM XRB Monitor

Bright transient events are removed from the data prior to fitting the background in preparation for the pulsar search. These events were cataloged for further analysis under the GBM XRB Monitor. The events are localized by using the angular response of the NaI detectors to reconstruct the most likely arrival direction based on the difference in the background subtracted count rates in the 12 NaI detectors which have different sky orientations. The method is adapted from the method used for GBM GRB localization (Connaughton et al. 2015). The XRB localization uses the 12–50 keV rates and spectral models appropriate for sources with softer energy spectra. Three cases are automatically identified: If the event localization is consistent with being toward the Sun then the event is identified as being solar, If the orientation of the bright detectors are inconsistent with a single direction then the event is identified as a particle event. Particle events tend to produce signal in all the detectors or in detectors with opposite orientation. If the event localization is consistent with a single direction and is not associated with the Sun then the event is considered a candidate XRB. These candidates undergo further analysis such as a refined localization and spectral analysis which occasionally resulted in a reclassification and rejection of the candidate status reducing the final number of XRBs to 1084. Using spectral analysis, location and spatial distributions we classified the 1084 events into

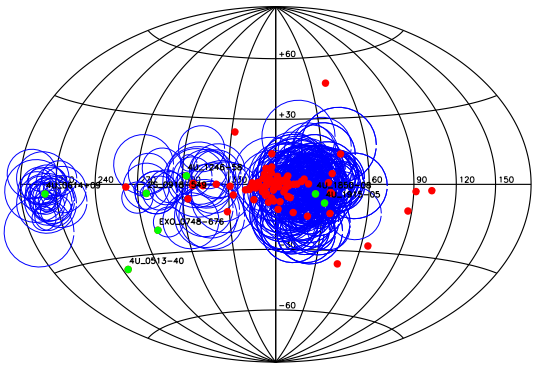

Fig. 9. The red and green filled circles are the know type 1 XRBs. The green filled circles are the XRBs that are sufficiently isolated from currently active sources that an association is possible. The blue circles are the GBM detected events. The radius of the circle is the approximate 1 sigma error region of the localization.

752 thermonuclear X-ray bursts (33 associated with 4U 0614+09), 267 transient events from accretion flares and X-ray pulses, and 65 untriggered gamma-ray bursts. See Figure 9 for the distribution of detected type 1 XRBs. All thermonuclear bursts have peak blackbody temperatures broadly consistent with photospheric radius expansion (PRE) bursts (Linares et al. 2012). We find an average rate of 1.4 PRE bursts per day, integrated over all Galactic bursters within about 10 kpc. These include 33 and 10 bursts from the ultra-compact X-ray binaries 4U 0614+09 and 2S 0918−549, respectively.

References

Case, G. L. et al. 2011, ApJ, 729, 105
Connaughton, V. et al. 2015, ApJs, 216, 32
Deeter, J. E. et al. 2003, ApJ, 247, 1003
Jenke, P. A. et al. 2016, ApJ, 826, 228
Jenke, P. A. et al. 2012, ApJ, 759, 124
Krimm, H. A. et al. 2013, ApJSS 209, 14
Linares, M. et al. 2012, ApJ, 760, 133
Matsuoka, M. et al. 2009, PASJ, 61, 999
Rappaport, S. and Joss, P. C. 1977, Nature, 266, 21
Standish, Jr., E. M. 1990, A&A, 233, 252
Townsend, L. J. et al. 2017, ArXiv e-prints, 1701.02336
Wilson-Hodge, C. A. et al. 2012, ApJS, 201, 33